International Journal of Heat and Mass Transfer 52 (2009) 2714–2720

Contents lists available at ScienceDirect

International Journal of Heat and Mass Transfer

journal homepage: www.elsevier.com/locate/ijhmt

Inverse problem of transpiration cooling for estimating wall heat flux by LTNE model and CGM method

Junxiang Shi, Jianhua Wang *

Department of Thermal Science and Energy Engineering, University of Science and Technology of China, Jinzhai Road No. 96, Hefei, Anhui 230027, PR China

ARTICLE INFO

Article history:
Received 28 August 2008
Received in revised form 20 December 2008
Available online 14 February 2009

Keywords:
Inverse problem
Transpiration cooling
Local thermal non-equilibrium model
Conjugate gradient method

ABSTRACT

In this work, a transient inverse problem of transpiration cooling is investigated in detail. The heat flux on the wall to be cooled is estimated by single point temperature measurement. The local thermal non-equilibrium (LTNE) model is utilized to describe the energy conservation of transpiration cooling process, and the conjugate gradient method (CGM) is extended to solve the inverse problem. The accuracy of the solutions of the inverse problem is examined through three given heat fluxes with given measurement errors. The examination shows that with the LTNE model and CGM, satisfactory solutions can be obtained. The influences of the variation in thermal properties, compressibility and the location of sensor on the accuracy of the solutions are analyzed. The analysis indicates that the variation in thermal properties and compressibility should be considered when a large temperature gradient exists, and the sensor location should be as close as possible to the hot wall. The inverse solutions obtained by the measurements of solid and fluid temperatures are compared. Through the comparison, it is found that using the solid temperature measurement as the input of the inverse problem is better than using the fluid temperature measurement.

1. Introduction

Transpiration cooling has been proven as an effective mechanism of heat dissipation by a lot of investigators. In most numerical investigations on transpiration cooling, the heat flux on the hot wall was a given value as one of boundary conditions. For example, Landis and Bowman [1] studied transpiration cooling performance of rocket nozzle, Wang et al. [2,3] analyzed the parameters to control ablation with transient transpiration cooling, Greuel et al. [4] discussed the transpiration cooling for protecting cryogenic liquid rocket engine, Wolfersdorf [5] studied the effect of coolant side heat transfer on transpiration cooling, these works were all limited in a given heat flux on the hot wall to be thermal protected. To apply these foregone investigations, it is necessary to find an effective approach to determine the heat flux on the hot boundary. Glass et al. [6] analyzed numerically the convection and transpiration cooling effect on the surface of a high temperature combustor, and solved the heat flux using a boundary layer code and a finite difference code of porous media. Haeseler et al. [7] investigated transpiration cooled hydrogen–oxygen subscale chamber through experiments and computations, in order to establish the heat flux profile over the chamber, they measured the average pressures and temperatures at the inlet and outlet of the chamber under static condition. However, in a practical transpiration cooling process, the heat flux is dependent on time, space, operation-state and coolant injection conditions, thus this is a transient inverse problem of enhanced heat exchange.

The inverse problems of heat transfer have been discussed by temperature measurements for a long time. Huang and Huang [8] determined simultaneously the spatial-dependent effective thermal conductivity and volumetric heat capacity of a biological tissue based on temperature measurements. Hong and Baek [9] estimated the unsteady inlet temperature distribution of the two-phase laminar flow in a channel by downstream temperature measurements. Huang [10] calculated the spatial-dependent wall heat flux of the laminar flow in a parallel plate duct through temperature measurements. Li and Yan [11] solved an inverse problem of the unsteady convection in an annular duct, and used temperature data to determine the time and space-dependent heat flux distribution on the inner wall of the duct. Chen et al. [12] calculated the time and space-dependent heat transfer rate on the external wall of a pipe system with temperature measurements. Lin et al. [13] investigated the heat flux of the unsteady laminar forced convection in parallel plate channels by temperature measurements. In recent years, some new methods were utilized to solve the inverse problems. Li and Yang [14] used the genetic algorithm (GA) for estimating the scattering albedo, optical thickness and phase function in parallel plane. Kim

* Corresponding author. Tel.: +86 551 3600945.
E-mail address: jhwang@ustc.edu.cn (J. Wang).

0017-9310/$ - see front matter © 2009 Elsevier Ltd. All rights reserved.
doi:10.1016/j.ijheatmasstransfer.2008.12.012

Nomenclature

y,Y	coordinate
m	coolant mass flow rate, kg/m^2 s
M	dimensionless coolant mass flow rate
V_f	dimensionless velocity
Q	dimensionless heat flux
q	heat flux at hot surface, W/m^2
h	interfacial convective coefficient, W/m^2 K
K	permeability, m^2
p	pressure, *Pa*
α_{sf}	specific surface area, m^{-1}
c	specific heat capacity, J/kg K
T	temperature, K
k	thermal conductivity, W/m K
H	thickness of entire structure, m
t	time, s
h_{sf}	volumetric convective coefficient, W/m^2 K
v_f	velocity, m/s
Bi	Biot number
Ma	Mach number
Re	Reynolds number
St	Stanton number

Greek symbols

ε	porosity
ρ	density, kg/m^3
τ	dimensionless time
μ	viscosity, N/s m^2
θ	dimensionless temperature

Subscripts

0	initial
a	ablation
c	coolant reservoir
e	effective
f	fluid
i	measurement times
ref	reference
s	solid

et al. [15] estimated wall emissivities with the hybrid genetic algorithm (HGA). Lee et al. [16] used the repulsive particle swarm optimization (PSO) for estimating the unknown radiative parameters. Park and Lee [17] utilized the Karhunen–Loeve Galerkin procedure to determine the space-dependent wall heat flux of the laminar flow inside a duct from the temperature measurements within the flow.

As mentioned above, these investigations were not aimed at the heat transfer within porous media or transpiration cooling, and in the references of [9–13], the assumptions of constant thermal properties and incompressible fluid were used. Therefore, it is necessary to consider whether these assumptions are suitable for transpiration cooling inverse problem. The inverse problem of the hot boundary is an important topic in the investigation on transpiration cooling, and the solving method of this problem is also different from that of the generally inverse problem as mentioned above [8–17], because transpiration cooling concerns two coupled energy balance equations for flowing fluid and solid matrix, respectively. This paper presents an approach to solve the inverse problem using real-time temperature measurements. The aim is to provide the investigators with a relatively comprehensive reference to understand the hot boundary performance of transpiration cooling process.

2. Physical model and mathematical equations

The physical model used in this work is sketched in Fig. 1. There is a porous matrix with a thickness of H, its one side is exposed to a severe heat flux of $q(t)$. To protect the matrix from the heat flux, a fluid coolant at a reservoir temperature of T_c is injected into the porous matrix with a mass flow rate of m. In this work, the Darcy law is used as the momentum equation of the coolant. For accurate estimation of the heat flux, the heat exchange between the coolant and matrix within pores is considered in this work, and the LTNE model is utilized [1–6]. Since the effective thermal conductivity ratio of the matrix to the fluid ($k_{s,e}/k_{f,e}$) is usually very large in transpiration cooling problems, the thermal diffusion of the coolant within the porous matrix can be neglected [2,5]. This physical model can be described by the following mathematical equations:

$$\text{Continuity equation}: \quad \varepsilon\frac{\partial \rho_f}{\partial t}+\frac{\partial}{\partial y}(\rho_f v_f)=0 \tag{1}$$

$$\text{Momentum equation}: \quad v_f=-\frac{K}{\mu}\frac{\partial p}{\partial y} \tag{2}$$

$$\text{Fluid energy equation}: \quad (\rho c)_{f,e}\frac{\partial T_f}{\partial t}+(\rho c v)_f\frac{\partial T_f}{\partial y}=h_{sf}a_{sf}(T_s-T_f) \tag{3}$$

$$\text{Solid energy equation}: \quad (\rho c)_{s,e}\frac{\partial T_s}{\partial t}=\frac{\partial}{\partial y}\left(k_{s,e}\frac{\partial T_s}{\partial y}\right)-h_{sf}a_{sf}(T_s-T_f) \tag{4}$$

Here, $k_{s,e}$ is the effective thermal conductivity of the solid matrix, $(\rho c)_{s,e}$ and $(\rho c)_{f,e}$ are the effective thermal capacity of the solid matrix and coolant fluid, respectively, they can be calculated by the porosity ε of the matrix:

$$k_{s,e}=(1-\varepsilon)k_s \tag{5}$$

$$(\rho c)_{f,e}=\varepsilon(\rho c)_f \tag{6}$$

$$(\rho c)_{s,e}=(1-\varepsilon)(\rho c)_s \tag{7}$$

The coolant fluid is assumed as perfect gas in this paper, and its density can be calculated as the following equation:

$$p=\rho_f R T_f \tag{8}$$

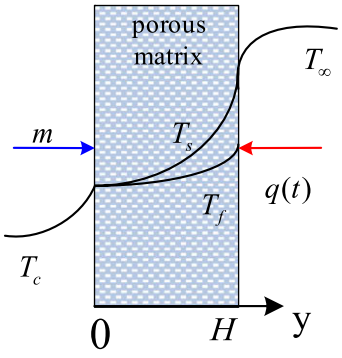

Fig. 1. Model of transpiration cooling.

At the initial time, the entire matrix is at the same temperature and pressure.

$$\begin{cases} T_s = T_f = T_0 \\ p = p_0 \end{cases} \quad t = 0,\ y \in [0, H] \tag{9}$$

On the cold side of the matrix, the boundary conditions suggested by [3,5] are used as:

$$\begin{aligned} h(T - T_c) &= k_{s,e}\frac{\partial T}{\partial y} \\ h(T_s - T_c) &= mc_f(T_f - T_c) \end{aligned} \tag{10}$$

On the hot side of the matrix, the boundary condition suggested by [2–3,5] is used as:

$$k_{e,s}\left.\frac{\partial T}{\partial y}\right|_{y=H} = q, \quad t > 0,\ y = H \tag{11}$$

To close this problem, the mass conservation law is applied as:

$$m = \rho_f v_f = \text{const} \tag{12}$$

Introducing the following dimensionless variables:

$$Y = \frac{y}{H}, \quad \theta = \frac{T - T_c}{T_{ref}}, \quad \bar{\rho}_f = \frac{\rho_f}{\rho_{f,ref}}, \quad P = \frac{p}{p_{ref}}, \quad V_f = \frac{v_f}{v_{f,ref}} \tag{13}$$

$$\tau = \frac{t}{H^2(\rho c)_{s,ref}/k_{s,ref}}, \quad M = \frac{Hmc_{f,ref}}{\varepsilon k_{f,ref}}, \quad Q = \frac{qH}{(1-\varepsilon)k_{s,ref}T_{ref}} \tag{14}$$

$$Bi = \frac{h_{sf}a_{sf}H^2}{(1-\varepsilon)k_{s,ref}}, \quad St = \frac{h_c}{(\rho v c)_{f,ref}}, \quad Re = \frac{Km_f}{H\mu}, \quad Ma = \frac{v_{f,ref}}{\sqrt{\gamma RT_{ref}}} \tag{15}$$

$$p_{ref} = p_{out}, \quad T_{ref} = T_a - T_c, \quad \rho_{f,ref} = p_{ref}/RT_{ref}, \quad v_{f,ref} = m_f/\rho_{f,ref} \tag{16}$$

Here, T_c is the coolant temperature in the reservoir, and T_a is the solid ablation temperature which is also allowable maximal temperature of the porous matrix. Thus, the dimensionless temperatures of the solid and fluid are within 0 and 1 limited. All of the initial thermal properties are taken at the initial temperature T_0. Using these dimensionless variables, the governing equations, initial and boundary conditions can be rewritten as the following dimensionless forms:

$$\frac{\partial \bar{\rho}_f}{\partial \tau} + M\frac{k_{f,ref}}{k_{s,ref}}\frac{\partial}{\partial Y}(\bar{\rho}_f V_f) = 0 \tag{17}$$

$$V_f = -\frac{1}{\gamma(Ma)^2}Re\frac{\partial P}{\partial Y} \tag{18}$$

$$\frac{\partial \theta_f}{\partial \tau} + V_f M\frac{(k/\rho c)_{f,ref}}{(k/\rho c)_{s,ref}}\frac{\partial \theta_f}{\partial Y} = Bi\frac{(\rho c)_{s,e,ref}}{(\rho c)_{f,e}}(\theta_s - \theta_f) \tag{19}$$

$$\frac{\partial \theta_s}{\partial \tau} = \frac{(\rho c)_{s,ref}}{(\rho c)_s}\frac{\partial}{\partial Y}\left(\frac{k_s}{k_{s,ref}}\frac{\partial \theta_s}{\partial Y}\right) - Bi\frac{(\rho c)_{s,ref}}{(\rho c)_s}(\theta_s - \theta_f) \tag{20}$$

$$P = \bar{\rho}_f\left(\theta_f + \frac{T_c}{T_a - T_c}\right) \tag{21}$$

$$\tau = 0, \quad Y \in [0,1]\ \theta_s = \theta_f = \theta_0, \quad P = P_0 \tag{22}$$

$$\tau > 0,\ Y = 0\begin{cases} \theta_f = St\theta_s \\ StM\frac{k_{f,e,ref}}{k_{s,e}}\theta_s = \frac{\partial \theta_s}{\partial Y} \\ \bar{\rho}_f V_f = 1 \end{cases} \tag{23}$$

$$\tau > 0,\ Y = 1\begin{cases} \frac{k_s}{k_{s,ref}}\frac{\partial \theta_s}{\partial Y} = Q \\ P = 1 \end{cases} \tag{24}$$

The direct problem (17)–(20) can be solved by the finite difference method on stagger mesh. It must be noted that when the thermal properties of coolant fluid and porous solid, such as thermal conductivity and capacity, are variable and temperature dependent, or the coolant fluid is compressible, the coefficients in non-linear equations (17)–(20) and boundary conditions (23) and (24) should be renewed in each iterative step.

3. Conjugate gradient method and numerical process

In the direct problem, the variations in the fluid and solid temperatures are calculated with certain initial and boundary conditions, and the heat flux on the hot surface is given as a boundary condition. In this inverse problem, the heat flux on the hot side $Q(\tau)$ is to be calculated by the temperature measurements. The solutions of the surface heat flux is approached by minimizing the object function as below:

$$J = \sum_{i=1}^{N}(\theta_i - Z_i)^2 \tag{25}$$

Here, $\theta_i(Y)$ is the dimensionless temperature obtained by calculation with an estimated $Q(\tau)$, $Z_i(Y)$ is the dimensionless temperature measured by a thermal sensor, N is the total number of measurement times in a given period of time. If $Y = 0$, the sensor measurement is at the cold side of the matrix. If $Y = 1$, the sensor measurement is at the hot side of the matrix. If $0 < Y < 1$, the sensor measurement is within the porous matrix.

The inverse problem is in an ill-posed, the estimated heat flux is very sensitive to the measurement errors, and the solution might not unique. However there are many applications of inverse problem in engineering. To obtain a stable solution, different mathematic methods, conjugate gradient method (CGM) [9–13], genetic algorithm (GA) [14,15], particle swarm optimization (PSO) [16] and Karhunen–Loeve Galerkin procedure (KLGP) [17] have been tried. In this work, the CGM is applied, because the CGM has a characteristic of quick convergence [12,16]. The heat flux is approximated by the following iterative process:

$$Q_n^{p+1} = Q_n^p - \beta^p d_n^p \tag{26}$$

Here, p is the number of iteration time, β^p and d_n^p is step size and descent direction, and can be calculated by

$$d_n^p = \left(\frac{\partial J}{\partial Q_n}\right)^p + \gamma^p d_n^{p-1} \tag{27}$$

$$\beta^p = \frac{\sum_{i=1}^{N}\left[(\theta_i^p - Z_i)\sum_{n=1}^{N}\left(\frac{\partial \theta_i}{\partial Q_n}\right)^p d_n^p\right]}{\sum_{i=1}^{N}\left[\sum_{n=1}^{N}\left(\frac{\partial \theta_i}{\partial Q_n}\right)^p d_n^p\right]^2} \tag{28}$$

In Eq. (27), γ^p is a conjugate coefficient, and can be determined by

$$\gamma^p = \frac{\sum_{n=1}^{N}\left[\left(\frac{\partial J}{\partial Q_n}\right)^p\right]^2}{\sum_{n=1}^{N}\left[\left(\frac{\partial J}{\partial Q_n}\right)^{p-1}\right]^2} \quad \gamma^0 = 0 \tag{29}$$

The gradient of the object function is calculated with Eq. (25):

$$\frac{\partial J}{\partial Q_n} = 2\sum_{i=1}^{N}(\theta_i - Z_i)\frac{\partial \theta_i}{\partial Q_n} \tag{30}$$

Here, $\partial\theta_i/\partial Q_n$ is the sensitivity coefficient which can be calculated through the energy equations (19) and (20). Considering variation

in the thermal properties with the temperature, the sensitivity coefficient equations and boundary conditions can be expressed as:

$$\frac{\partial(\rho c)_{f,e}}{(\rho c)_{f,e}\partial\theta_f}\frac{\partial\theta_f}{\partial Q_n}\frac{\partial\theta_f}{\partial\tau}+\frac{\partial}{\partial\tau}\left(\frac{\partial\theta_f}{\partial Q_n}\right)+V_f M\frac{(k/\rho c)_{f,ref}}{(k/\rho c)_{s,ref}}\frac{\partial(\rho c)_{f,e}}{(\rho c)_{f,e}\partial\theta_f}\times\frac{\partial\theta_f}{\partial Q_n}\frac{\partial\theta_f}{\partial Y}+V_f M\frac{(k/\rho c)_{f,ref}}{(k/\rho c)_{s,ref}}\frac{\partial}{\partial Y}\left(\frac{\partial\theta_f}{\partial Q_n}\right)=Bi\frac{(\rho c)_{s,e,ref}}{(\rho c)_{f,e}}\left(\frac{\partial\theta_s}{\partial Q_n}-\frac{\partial\theta_f}{\partial Q_n}\right) \tag{31}$$

$$\frac{\partial(\rho c)_s}{(\rho c)_s\partial\theta_s}\frac{\partial\theta_s}{\partial Q_n}\frac{\partial\theta_s}{\partial\tau}+\frac{\partial}{\partial\tau}\left(\frac{\partial\theta_s}{\partial Q_n}\right)=\frac{(\rho c)_{s,ref}}{(\rho c)_s}\frac{\partial}{\partial Y}\left(\frac{1}{k_{s,ref}}\left(\frac{\partial k_s}{\partial\theta_s}\frac{\partial\theta_s}{\partial Q_n}\frac{\partial\theta_s}{\partial Y}+k_s\frac{\partial}{\partial Y}\left(\frac{\partial\theta_s}{\partial Q_n}\right)\right)\right)-Bi\frac{(\rho c)_{s,ref}}{(\rho c)_s}\left(\frac{\partial\theta_s}{\partial Q_n}-\frac{\partial\theta_f}{\partial Q_n}\right) \tag{32}$$

$$\frac{\partial\theta_s}{\partial Q_n}=\frac{\partial\theta_f}{\partial Q_n}=0\quad\tau=0,\ Y\in[0,1] \tag{33}$$

$$\begin{cases} StM\frac{k_{f,e,ref}}{k_{s,e}}\left(\frac{\partial\theta_s}{\partial Q_n}\right)=\frac{\partial k_{s,e}}{k_{s,e}\partial\theta_s}\frac{\partial\theta_s}{\partial Q_{m,n}}\frac{\partial\theta_s}{\partial Y}+\frac{\partial}{\partial Y}\left(\frac{\partial\theta_s}{\partial Q_{m,n}}\right) \\ \frac{\partial\theta_f}{\partial Q_n}=St\frac{\partial\theta_s}{\partial Q_n}\end{cases}\quad\tau>0,\ Y=0 \tag{34}$$

$$\frac{1}{k_{s,ref}}\left(k_s\frac{\partial}{\partial Y}\left(\frac{\partial\theta_s}{\partial Q_{m,n}}\right)+\frac{\partial k_s}{\partial\theta_s}\frac{\partial\theta_s}{\partial Q_{m,n}}\frac{\partial\theta_s}{\partial Y}\right)=\hat{u}(\tau-\tau_n)\quad\tau>0,\ Y=1 \tag{35}$$

Here,

$$\hat{u}(\tau-\tau_n)=\begin{cases}1 & \text{if } \tau=\tau_n\\ 0 & \text{otherwise.}\end{cases}$$

When the thermal properties are independent of the temperatures, the values of $\frac{\partial(\rho c)_{f,e}}{\partial\theta_f}$, $\frac{\partial(\rho c)_s}{\partial\theta_s}$, $\frac{\partial k_s}{\partial\theta_s}$ and $\frac{\partial k_{s,e}}{\partial\theta_s}$ would be zero, Eqs. (31) and (32) can be solved by the same approach referred to direct problem (19) and (20) previously.

When the thermal properties are temperature dependent or the fluid is compressible, non-linear equations (31) and (32) are more complicated than Eqs. (19) and (20), because the coefficients in the equations and boundary conditions will vary with measure time, the values of V_f, $\frac{\partial\theta_i}{\partial\tau}$ and $\frac{\partial\theta_i}{\partial Y}$ $(i=s,f)$ have been known in previous calculation step, and the values of $\frac{\partial(\rho c)_{f,e}}{\partial\theta_f}$, $\frac{\partial k_s}{\partial\theta_s}$ and $\frac{\partial k_{s,e}}{\partial\theta_s}$ have to be renewed in each iterative step. The non-linear equations are numerically solved with the finite difference approach, and the sensitivity $\frac{\partial\theta}{\partial Q_n}$ is renewed in each measurement time step.

If there is no any measurement errors in the inverse problem, the iteration stopping criterion is $J<\sigma$, and in this paper σ is 10^{-5}. If there is a random error with a standard deviation of η in the measurement data, the stopping criterion is modified as:

$$J<N\eta^2 \tag{36}$$

The computational procedure for the inverse problem of transpiration cooling can be expressed with the following steps:

Step 1. Using a guess heat flux $Q_n^0=0$, solving Eqs. (17)–(20), to obtain the temperature field θ_i by the method of direct problem.
Step 2. Calculating the objective function J through Eq. (25), if the stopping criterion is satisfied, the iteration procedure is terminated, otherwise goes to step 3.
Step 3. Solving sensitivity equations (31) and (32), to obtain the sensitivity coefficient $\frac{\partial\theta_i}{\partial Q_n}$
Step 4. Using $\frac{\partial\theta_i}{\partial Q_n}$, $\theta_{i,j}$ and $Z_{i,j}$, to calculate $\frac{\partial J}{\partial Q_n}$ with Eq. (30), γ^p with Eq. (29), d_n^p with Eq. (27) and β^p with Eq. (28).

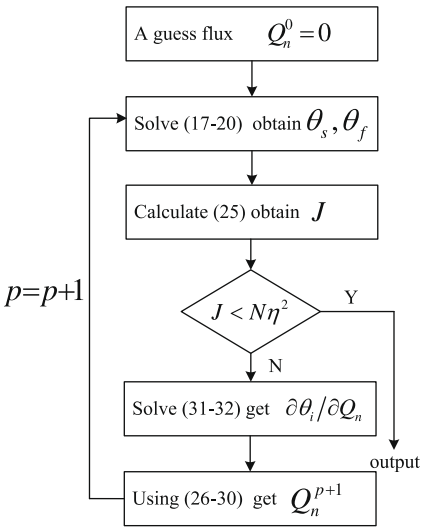

Fig. 2. Computational procedure of CGM for the inverse problem of transpiration cooling.

Step 5. Using d_n^p and β^p, to calculate Q_n^{p+1} by Eq. (17), setting $p=p+1$ and going to step 2 (Fig. 2).

4. Results and discussion

To estimate the accuracy of the presented approach, the following three kinds of heat flux functions are used as the given hot boundary condition:

$$\text{G1 } Q(\tau)=20abs\left(\sin\left(\frac{\pi\tau}{0.18}\right)\right)\quad\tau\in[0,0.36] \tag{37}$$

$$\text{G2 } Q(\tau)=10+10\cos\left(\frac{\pi\tau}{0.18}\right)\quad\tau\in[0,0.36] \tag{38}$$

$$\text{G3 }\begin{cases}Q(\tau)=20(0.36-\tau) & 0\leqslant\tau\leqslant0.18\\ Q(\tau)=20\tau & 0.18<\tau\leqslant0.36\end{cases} \tag{39}$$

To consider the variations in the thermal properties and compressibility, the following fitting relations are used:

$$k_s\ (\text{W/m K})=7.86+1.73\times10^{-2}T-1.50\times10^{-5}T^2+9.14\times10^{-9}T^3 \tag{40}$$

$$k_f\ (\text{W/m K})=5.49\times10^{-2} \tag{41}$$

$$c_{ps}\ (\text{J/kg K})=422.69+0.26T-3.22\times10^{-4}T^2+1.92\times10^{-7}T^3 \tag{42}$$

$$c_{pf}\ (\text{J/kg K})=1029.18-0.23T+5.86\times10^{-4}T^2-2.45\times10^{-7}T^3 \tag{43}$$

The other parameters are taken as below:

$$\rho_s\ (\text{kg/m}^3)=7860,\quad T_a\ (\text{K})=1250,\quad T_c\ (\text{K})=T_0\ (\text{K})=293,\quad H\ (\text{m})=0.05 \tag{44}$$

$$\mu\ (\text{N s/m}^2)=1.0E-5,\quad K\ (\text{m}^2)=1.0E-5,\quad p_{out}\ (\text{Pa})=p_0\ (\text{Pa})=1.0E5 \tag{45}$$

$$\varepsilon=0.15,\quad Bi=5.0E2,\quad Stc=1,\quad Pr=0.8,\quad M=5.0E4 \tag{46}$$

The measured temperature data Z are generated by adding random errors to the exact temperature data θ which are calculated from the solutions of the given heat flux:

$$Z = \theta + \eta\xi$$

Here, η is a standard deviation, and ξ is a random variable within −2.576 to 2.576 within 99% confidence bound.

In order to keep undisturbed flow field, in this paper, the thermal sensors are assumed to be embedded within the porous solid, and the measurement location is at the hot surface $Y = 1$. That means $\theta_{s,i}$ and $\frac{\partial\theta_{s,i}}{\partial Q_n}$ are seen to be θ_i and $\frac{\partial\theta_i}{\partial Q_n}$, respectively.

4.1. Validation of inverse solutions

Fig. 3 illustrates a comparison between the three given heat fluxes G1, G2, G3 and the corresponding inverse solutions obtained by $\eta = 0$. It is clear that the inverse solutions are in well agreement with the given values.

Fig. 4 compares the three given heat fluxes with the inverse solutions obtained by a standard deviation of 0.5%. It can be found that although there is a measurement error, the inverse solutions obtained by the CGM are satisfactory.

Through above two comparisons, the inverse method with CGM in this paper can essentially be confirmed to be valid.

4.2. Effects of variable thermal properties and fluid compressibility

Fig. 5 shows the influences of the variation in thermal properties and coolant density on the inverse solutions. It can be found that under the assumption of constant thermal properties, two heat fluxes, one is of compressible fluid, and the other is of incompressible fluid, are obviously lower than the given boundary condition G1. Whereas under the condition of variable thermal properties, the inverse solutions obtained by the assumption of incompressibility are higher than the G1. These results are reasonable, because if the thermal conductivity and heat capacity are variable, they would increase with the temperature, according to the Eqs. (40)–(43), therefore, under the same heat flux, the solutions of the direct problem with variable thermal properties can obtain lower temperatures than that with constant thermal properties. On the other hand, when the coolant fluid is compressible, the fluid velocity within the porous matrix is larger than that in incompressible case, under the same heat flux, more quantity of the heat absorbed by the matrix can be transported by the coolant flow, therefore the solutions of the direct problem with compressibility can obtain lower temperature than that with incompressibility. From these comparisons, it can be found that the variation in thermal properties and fluid density should be considered in the inverse problem of the transpiration cooling with large temperature gradients.

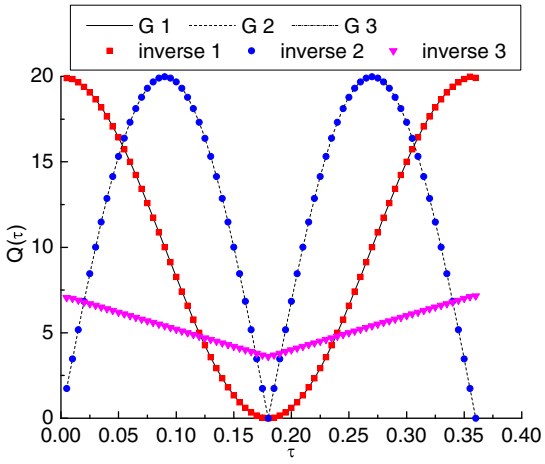

Fig. 3. Inverse solutions with three case heat flux formulation and no measure errors.

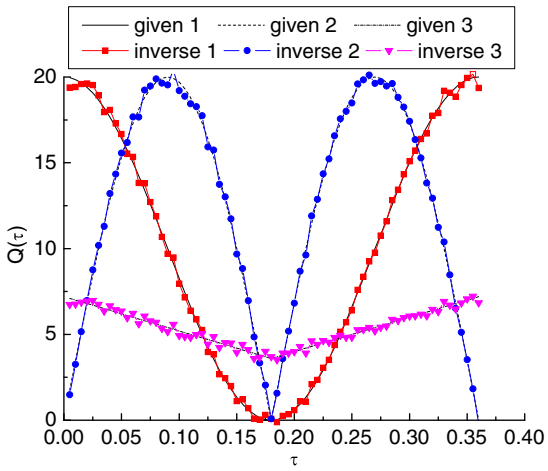

Fig. 4. Inverse solutions with standard deviation 0.5% and $N = 72$.

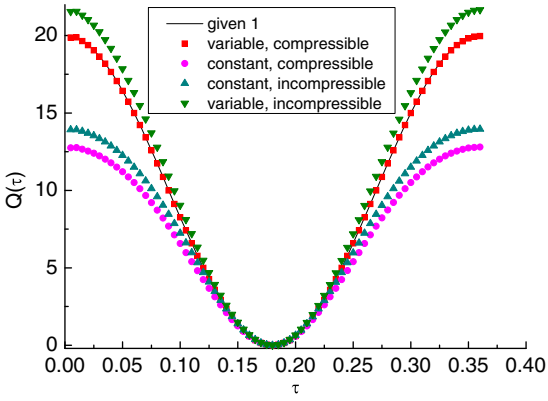

Fig. 5. Effect of thermal properties and compressibility on the inverse solution.

4.3. Effects of measurement times N

To analyze the influence of measurement times N on the solutions, an absolute average error in the estimated heat flux is defined as below:

$$f_{err} = \frac{1}{N}\sum_{i=1}^{N}\left|Q_i^g - Q_i^e\right| \tag{47}$$

Here, Q_i^g is the given heat flux G1, Q_i^e is the heat flux obtained by the measured temperature with given standard deviations 0.5% and 1%, and the total measurement times N are multiples of nine, $9 \times k$ ($k = 1 \ldots 16$).

Fig. 6 illustrates the influence of the measurement times on the inverse solutions. The absolute average errors decrease observably with an increase in the measurement times from 9 to 63, but from 63 to 144, the changes in the absolute average errors are not significant, though some slightly fluctuations appear, these fluctuations can be deemed to be caused by increased computational errors. It is well known that the computational time and memory are also increased with the measurement times. Considering this phenomenon, the following solutions are obtained by 72 measurement times.

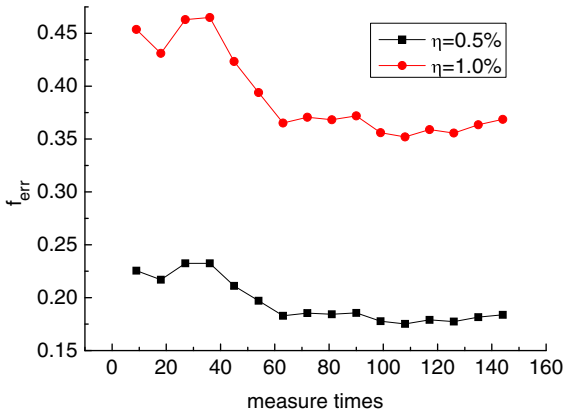

Fig. 6. Relationship of absolute average error with measurement times.

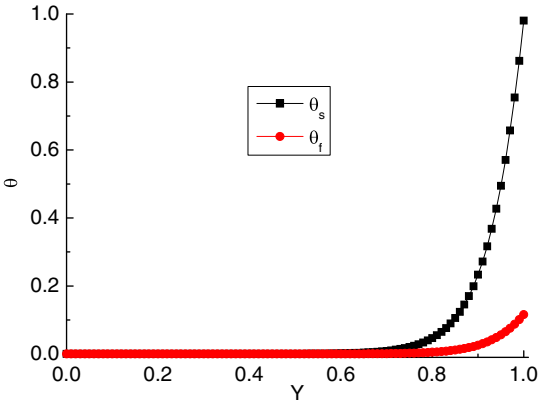

Fig. 8. Temperature distribution in porous matrix of transpiration cooling.

4.4. Effects of measurement location

Fig. 7 illustrates the influence of measurement location Y on the solutions of the inverse problem, when the standard deviation is at 0.5%. It is clear that a farther location away from the hot surface corresponds to a larger deviation from the given heat flux. This phenomenon can be explained by Fig. 8. The fluid and solid temperature distributions within the matrix in Fig. 8 are obtained at a certain heat flux of $Q = 20$. It can be observed that in the region from $Y = 0$ to 0.8, the temperatures of the two phases are close to 0. Obviously, the measurement temperature in the region from 0 to 0.8 can not be used as the input of the inverse problems, because the temperatures in this region are very close to coolant reservoir temperature, and not sensitive to the heat flux at the hot surface. From 0.8 to 1, the temperatures of solid and fluid increase quickly, and in this region, the effect of the boundary heat flux is stronger than that of the reservoir. Therefore, the measurement location in the inverse problems should be as close as possible to the hot surface.

4.5. Effects of solid and fluid temperature measurements

If the temperatures of coolant fluid and solid matrix can be measured separately, which temperature as the input of the inverse problems is better? To answer this question, a numerical comparison is performed. Under the given heat flux G1, the fluid and solid temperatures on the hot surface can be obtained. If the fluid and solid temperatures added by the same deviation of 0.5% are used as the input of the inverse problems, two different heat flux profiles can be obtained, as shown in Fig. 9. It is clear that the inverse solutions obtained by the solid temperature are more close to the given value G1 at all. This phenomenon is reasonable, in this paper and foregone investigations [2,5] the thermal conductivity of the solid is much larger than that of the fluid, the temperature increase of the fluid depends mainly on the convective heat transfer with the porous solid, therefore the solid temperature is much more sensitive to the heat flux, as shown in Fig. 8. From this phenomenon, one can obtain a conclusion: it is better using the solid temperature as the input of the inverse problem than the fluid temperature when the thermal conductivity of the solid is larger than that of the fluid. In actual fact, considering the disturbance of thermal sensors on the fluid flow field, the measurement of coolant temperature is not recommended.

5. Conclusion

An inverse problem of transpiration cooling for estimating the time-dependent heat flux has been numerically discussed in this work. The local thermal non-equilibrium model and conjugate gradient method are used to solve the inverse problem. Through this investigation, the following conclusions can be drawn:

- The local thermal non-equilibrium model and conjugate gradient method, as an effective approach, can be applied to estimate the heat flux on the hot surface to be protected by transpiration cooling.
- In the inverse problem solutions of transpiration cooling, the assumption of constant thermal conductivity and capacity will lead to an underestimated heat flux, and incompressibility will

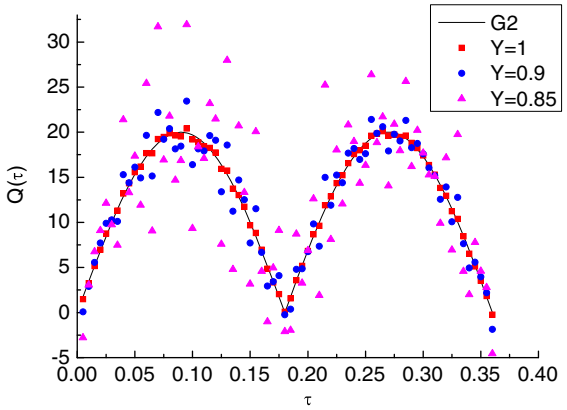

Fig. 7. Inverse solutions with three sensor position and standard deviation 0.005.

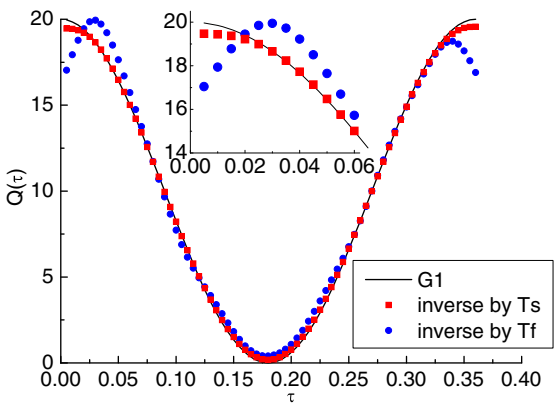

Fig. 9. Inverse solutions with the measurement of different phase.

lead to an overestimated heat flux. Therefore, the variations in the thermal properties and fluid compressibility should be considered, especially in the transpiration cooling problems with a large temperature gradient.

- As the input of the inverse problem, the solid temperature measurement is better than the fluid temperature measurement when the thermal conductivity of the solid is larger than that of the fluid.
- The measurement location of the solid temperature should be as close as possible to the hot surface.

Acknowledgements

The project is supported by National Natural Science Foundation of China (No. 90305006 and No. 10772175). One of the authors (Jianhua Wang) is also grateful for the financial support provided by the Foundation of the Education Ministry of China for the Returned Overseas Scholars.

References

[1] J.A. Landis, J.W. Bowman, Numerical study of a transpiration cooled rocket nozzle [R], AIAA Meeting, Paper 96-2580, 1996.
[2] H.N. Wang, J.H. Wang, A numerical investigation of ablation and transpiration cooling using the local thermal non-equilibrium model [R], in: Proceeding of the 42nd AIAA/ASME/SAE/ASEE Joint Propulsion Conference & Exhibit, Sacramento, California, July 9–12, AIAA-2006-5264, 2006.
[3] J.H. Wang, H.N. Wang, J.G. Sun, J. Wang, Numerical simulation of control ablation by transpiration cooling, Heat Mass Transfer 43 (2007) 471–478.
[4] D. Greuel, A. Herbertz, O.J. Haidn, M. Ortelt, H. Hald, Transpiration cooling applied to C/C liners of cryogenic liquid rocket engines [R], AIAA 2004-3682.
[5] J.V. Wolfersdorf, Effect of coolant side heat transfer on transpiration cooling, Heat Mass Transfer 41 (2005) 327–337.
[6] David E. Glass, Arthur D. Dilley, H. Neale Kelly, Numerical analysis of convection transpiration cooling [R], NASA/TM-1999-209828.
[7] D. Haeseler, C. Mading, V. Rubinskiy, V. Gorokhov, S. Khrisanfov, Experimental investigation of transpiration cooled hydrogen–oxygen subscale chambers [R], AIAA 98-3364.
[8] Cheng-Hung Huang, Chu-Ya Huang, An inverse problem in estimating simultaneously the effective thermal conductivity and volumetric heat capacity of biological tissue, Appl. Math. Model. 31 (2007) 1785–1797.
[9] Yun Ky Hong, Seung Wook Baek, Inverse analysis for estimating the unsteady inlet temperature distribution for two-phase laminar flow in a channel, Int. J. Heat Mass Transfer 49 (2006) 1137–1147.
[10] Ch Huang, Inverse problem of determining unknown wall heat-flux in laminar-flow through a parallel plate duct, Numer. Heat Transfer A 21 (1992) 55–70.
[11] H.-Y. Li, W.-M. Yan, Inverse convection problem for determining wall heat flux in annular duct flow, ASME J. Heat Transfer 122 (2000) 460–464.
[12] Wen-Lih Chen, Yu-Ching Yang, Win-Jin Chang, Haw-Long Lee, Inverse problem of estimating transient heat transfer rate on external wall of forced convection pipe, Energy Convers. Manage. 49 (2008) 2117–2123.
[13] D.T.W. Lin, W.M. Yan, H.Y. Li, Inverse problem of unsteady conjugated forced convection in parallel plate channels, Int. J. Heat Mass Transfer 51 (2008) 993–1002.
[14] H.Y. Li, C.Y. Yang, A genetic algorithm for inverse radiation problems, Int. J. Heat Mass Transfer 40 (1997) 1545–1549.
[15] K.W. Kim, S.W. Baek, M.Y. Kim, H.S. Ryu, Estimation of emissivities in a two-dimensional irregular geometry by inverse radiation analysis using hybrid genetic algorithm, J. Quant. Spectrosc. Radiat. Transfer 87 (2004) 1–14.
[16] Kyun Ho Lee, Seung Wook Baek, Ki Wan Kim, Inverse radiation analysis using repulsive particle swarm optimization algorithm, Int. J. Heat Mass Transfer 51 (2008) 2772–2783.
[17] H.M. Park, J.H. Lee, A method of solving inverse convection problem by means of mode reduction, Chem. Eng. Sci. 53 (1998) 1731–1744.